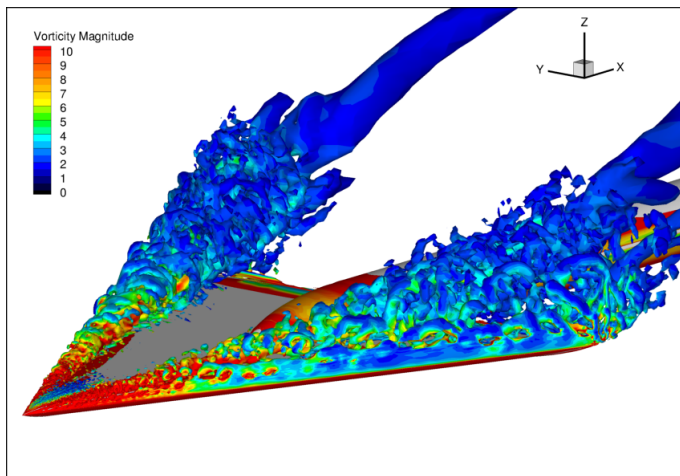




Executive summary

Capturing free shear layers in hybrid RANS–LES simulations of separated flow



Problem area

Massively separated flows play an important role in topics such as the design of silent landing gear, the study of stability and control properties of fighter aircraft in relation to vortex breakdown, and the study of aerodynamic loads on structural aircraft components due to buffeting. These flows are strongly turbulent, involving a large range of spatial and temporal scales, which makes it difficult to model their dynamics with high physical accuracy and reliability. Flow computations based on the Reynold-averaged Navier–Stokes (RANS) equations are not able to capture the smaller turbulent scales. Large-eddy simulations (LES), on the other hand, do capture a significant range of

scales, but are computationally too demanding for complex geometries. In recent years, therefore, research has focussed on hybrid RANS–LES methods, improving the physical accuracy compared to RANS, but without the cost of a full LES. In particular, NLR has developed the eXtra-Large Eddy Simulation (X-LES) method.

Description of work

An important issue in hybrid RANS–LES methods is the capturing of free shear layers. Typically, free shear layers are present between the attached boundary layers (computed with RANS) and the separated flow regions (computed with LES). These shear layers may develop too slowly in X-LES and

Report no.

NLR-TP-2012-333

Author(s)

J.C. Kok and H. van der Ven

Classification report

Unclassified

Date

August 2012

Knowledge area(s)

Computational Physics &
Theoretical Aerodynamics

Descriptor(s)

Hybrid RANS–LES
Free shear layer
DES
Subgrid-scale model
High-order method

similar hybrid RANS–LES methods, which may influence the extent of the separated flow regions. To improve the capturing of free shear layers, two modifications have been considered: a stochastic subgrid-scale (SGS) model and a high-pass filtered SGS model.

Results and conclusions

The two considered modifications of X-LES substantially improve the development of free shear layers. The stochastic SGS model triggers shear-layer instabilities. The high-pass filtered SGS model ensures that the shear layer exhibits the cor-

rect growth rate. Finally, numerical methods must be carefully designed in order to accurately capture free shear layers without numerical errors overwhelming the subgrid stresses.

Applicability

Free shear layers appear in many applications, for example, vortical flows around fighter aircraft or landing gear wakes, and strongly influence the downstream flow development. For all these applications, the improvements of the X-LES method are relevant and may improve the computational results.



NLR-TP-2012-333

Capturing free shear layers in hybrid RANS-LES simulations of separated flow




J.C. Kok and H. van der Ven

This report is based on an invited lecture held at the Second Symposium "Simulation of Wing and Nacelle Stall", 21-22 June 2012, Braunschweig, Germany.

The contents of this report may be cited on condition that full credit is given to NLR and the authors.
This publication has been refereed by the Advisory Committee AEROSPACE VEHICLES.

Customer	National Aerospace Laboratory NLR
Contract number	----
Owner	National Aerospace Laboratory, NLR
Division NLR	Aerospace Vehicles
Distribution	Unlimited
Classification of title	Unclassified
	August 2012

Approved by:

Author	Reviewer	Managing department
 6/8/2012	 8/8/2012	 8/8/2012

Summary

An important issue in Detached Eddy Simulations (DES) of separated flow is the capturing of free shear layers. Typically, free shear layers are present between the attached boundary layers (computed with RANS) and the separated flow regions (computed with LES). The turbulence in these shear layers may develop too slowly in DES, which may influence the extent of the separated flow regions. In this paper, the capturing of free shear layers in DES-type methods is substantially improved with two modifications: a stochastic subgrid-scale model and a high-pass filtered subgrid-scale model. Furthermore, it is shown that the numerical methods must be carefully designed in order to accurately capture free shear layers without numerical errors overwhelming the subgrid stresses.

Contents

Abbreviations	5
1 Introduction	7
2 Improvements of the X-LES method	8
3 Numerical method	10
3.1 A low-dispersion symmetry-preserving finite-volume method	10
3.2 Artificial diffusion	10
3.3 Time integration	12
4 Results	13
4.1 Plane free shear layer	13
4.2 Delta wing with sharp leading edge	15
5 Conclusions	19
References	20

Abbreviations

DES	Detached Eddy Simulation
DDES	Delayed Detached Eddy Simulation
DRP	Dispersion-Relation Preserving
HPF	High-Pass Filter
RANS	Reynolds-Averaged Navier–Stokes (equations)
SGS	Sub-Grid Stress
X-LES	Extra-Large Eddy Simulation



This page is intentionally left blank.

1 Introduction

Stall is a prime example of massively separated flow. Detached Eddy Simulation (DES) (Ref. 18) has been specifically designed to improve the simulation of separated flow compared to RANS. In DES, attached boundary layers are modelled with RANS, while massively separated flow is modelled with LES. Despite considerable success an important drawback of the method is the so-called ‘grey area’ issue: the transition from RANS to LES may lead to non-physical solutions as the turbulent content in the LES region requires time to develop. This phenomenon occurs in particular for free shear layers, resulting in the delay of the inherent instabilities. The resulting shear layer will exhibit laminar characteristics, even for turbulent conditions. Note that shear layers are abundant in separated flow and that the nature of the shear layer determines the extent of the separated region for many applications.

The grey area issue has been identified early in the development of DES methods (see e.g. Spalart (Ref. 17)). Specifically for the non-physical stability of the shear layer, four possible causes can be identified:

- Cause 1: The turbulence model remains in RANS mode.
- Cause 2: The unstable modes in the shear layer are not triggered, due to lack of turbulent content.
- Cause 3: The subgrid stresses (SGS) are too high.
- Cause 4: Numerical errors are too high, numerical dissipation in particular.

Several solution strategies have been proposed in the literature, each addressing one of the possible causes listed above:

- Cause 1: Zonal methods, such as proposed by Deck (Ref. 2), explicitly assign domains to be solved in LES mode and hence avoid the first cause.
- Cause 2: Moreover, when using fixed interfaces between RANS and LES zones, the use of synthetic turbulence (e.g., references 2, 7) at the interface will add turbulent content to the shear layer and speed up the instabilities. Kok *et al.* (Ref. 10) introduced a stochastic SGS model in their non-zonal DES-type X-LES method (Ref. 9) with the specific aim of triggering the instabilities by stochastic excitation.
- Cause 3: For LES computations of jet noise, Shur *et al.* (Ref. 15) have switched off the SGS model entirely to speed up the formation of instabilities. In his zonal method, Deck significantly reduced the subgrid stresses in the initial shear layer by using an alternative definition for the length scale used in the subgrid eddy viscosity.
- Cause 4: Shur *et al.* (Ref. 16) have introduced a hybrid numerical scheme which switches to a central, non-dissipative, high-order scheme in the LES zones. Kok (Ref. 8) has devel-

oped a central, fourth-order, symmetry-preserving finite-volume scheme with low dispersion and dissipation aimed at the LES regions of DES-type computations.

Zonal methods and the addition of synthetic turbulence typically require knowing *a priori* the location where the shear layer separates. In contrast, solution strategies are considered in the current paper that do not require this *a priori* knowledge, maintaining the original non-zonal spirit of the DES idea.

In the opinion of the authors, triggering the instabilities with a stochastic SGS model in combination with a reduction of the subgrid stresses using a high-pass filtered (HPF) SGS model is an effective way to speed up the development of free shear layers towards full 3D turbulence, provided carefully designed numerical methods with low dispersion and dissipation are used. This will be demonstrated in the remainder of this paper. In Section 2 the stochastic and HPF SGS models are described that improve the prediction of free shear layers. In Section 3 important aspects of the numerics for hybrid RANS–LES simulations are discussed. In Section 4 the effects of both numerics and modelling are demonstrated for two test cases: the plane free shear layer and a delta wing in vortex breakdown conditions.

2 Improvements of the X-LES method

In DES-type methods such as X-LES (Ref. 9), a single set of turbulence-model equations is used to model both the Reynolds stresses in RANS zones and the subgrid stresses in LES zones. The X-LES method in particular is based on the TNT k – ω model. The method switches to LES when the RANS length scale ($l = \sqrt{k}/\omega$) exceeds the LES length scale ($C_1\Delta$, with Δ the filter width and $C_1 = 0.05$). The RANS length scale is then replaced by the LES length scale in the expression for the eddy viscosity as well as in the expression for the dissipation of turbulent kinetic energy. The filter width Δ is defined at each grid point as the maximum of the mesh size in all directions.

To improve the capturing of free shear layers, two modifications have been added to the X-LES method. The first modification consists of a stochastic SGS model (Ref. 10), in which a stochastic variable $\xi = N(0, 1)$ is introduced in the expression for the eddy viscosity in LES mode. For the X-LES method, the expression for the eddy viscosity then becomes:

$$\nu_t = \begin{cases} k/\omega & , \text{ if } l \leq C_1\Delta, \\ \xi^2 C_1 \Delta \sqrt{k} & , \text{ if } l > C_1\Delta. \end{cases} \quad (1)$$

At each time step, a new value of ξ is drawn for every grid cell. The stochastic term is *not* included in the turbulent dissipation, which is given by

$$\varepsilon = \frac{\beta k^{3/2}}{\min\{l, C_1 \Delta\}} \quad (2)$$

with $\beta = 0.09$. Note that effectively a k -equation SGS model is used in LES zones (where $l > C_1 \Delta$), as ω drops out of the expressions for ν_t and ε .

The second modification consists of a high-pass filtered (HPF) SGS model. A possible source of dissipation hampering the shear-layer development is a high level of subgrid stresses in the initial shear layer. These high stresses are caused by a high gradient of the mean velocity field due to the initial shear layer being very thin. However, there is no apparent reason why the subgrid stresses should be related to this mean flow gradient. Therefore, a modification of the SGS model is also considered in which the SGS stresses are computed from the velocity fluctuations instead of the instantaneous velocity,

$$\tau_{ij} = \mu_t \left(\frac{\partial u'_i}{\partial x_j} + \frac{\partial u'_j}{\partial x_i} - \frac{2}{3} \frac{\partial u'_k}{\partial x_k} \delta_{ij} \right) - \frac{2}{3} \rho k \delta_{ij}. \quad (3)$$

The velocity fluctuations u' are obtained by applying a temporal high-pass filter to the velocity field. This high-pass filter consists of subtracting the running time average of the velocity from the instantaneous velocity:

$$u'(x, t) = u(x, t) - \frac{1}{t} \int_0^t u(x, s) ds. \quad (4)$$

A similar approach has been followed by Stolz (Ref. 19) and by L  v  que *et al.* (Ref. 14) using a spatial filter instead of a temporal filter in order to improve the Smagorinsky model for LES of wall-bounded flows. High-pass filters have also been used in the context of the structure-function model (Ref. 13).

The HPF SGS model has two additional advantages:

- In case of a steady, laminar flow (e.g., a laminar boundary layer), the subgrid stresses are zero, as they should be.
- At the start of a computation ($t = 0$) the velocity fluctuations as defined above are set to zero, so that the subgrid stresses are initially equal to zero. Thus, instabilities are initially not damped at all by the SGS model, allowing a shorter transient of the computations.

Note that both the stochastic SGS model and the HPF SGS model can also be employed in other DES-type methods.

3 Numerical method

3.1 A low-dispersion symmetry-preserving finite-volume method

For large eddy simulations, the spatial and temporal discretization methods must be chosen with care. For example, if the convection terms are discretized with standard second-order schemes (as commonly used for RANS), the resulting numerical errors can be of the same order of magnitude as the subgrid stresses (see Kravchenko and Moin (Ref. 11)). In that case, the computational results are determined as much by the numerical errors as by the SGS model.

To minimize the interference of numerical errors with the SGS model, the numerical accuracy of the scheme should be high at wave lengths close to the filter width. These wave lengths are represented by only a few mesh widths. Thus, what is important is the numerical error at a fixed, relatively large mesh width compared to the wave length, and not the formal order of accuracy of the scheme as the mesh width goes to zero. Numerical schemes optimized in that sense are, for example, the DRP scheme of Tam and Webb (Ref. 20) and the compact schemes of Lele (Ref. 12).

In this paper, a fourth-order, symmetry-preserving, low-dispersion finite-volume scheme as described by Kok (Ref. 8) is used to discretize convection. A central (instead of upwind) discretization is used, so that the method contains no numerical dissipation. The finite-volume method maintains its properties (fourth-order accurate, low numerical dispersion, no numerical dissipation) on non-uniform, curvilinear grids. On uniform, Cartesian grids, it is equivalent to the DRP scheme.

The superiority of the current, low-dispersion finite-volume scheme in terms of numerical dispersion, compared to basic fourth-order and second-order central schemes (see reference 8 for their definition), is shown in Figure 1(a). This figure shows the dispersion error for the spatial discretization of a linear, first-order transport equation using Fourier analysis. The error in the phase of a single Fourier mode after one time period is plotted versus the number of grid cells per wave length of the mode. With eight cells per wave length, the low-dispersion (DRP) scheme has a phase error of only 0.4° , whereas the standard fourth-order scheme has a phase error of 9° and the standard second-order scheme as large as 36° .

3.2 Artificial diffusion

As the present finite-volume method contains no numerical dissipation, a question that remains is whether any artificial diffusion is needed for stability. An important property of the symmetry-preserving finite-volume method is that it ensures that kinetic energy is conserved by convection

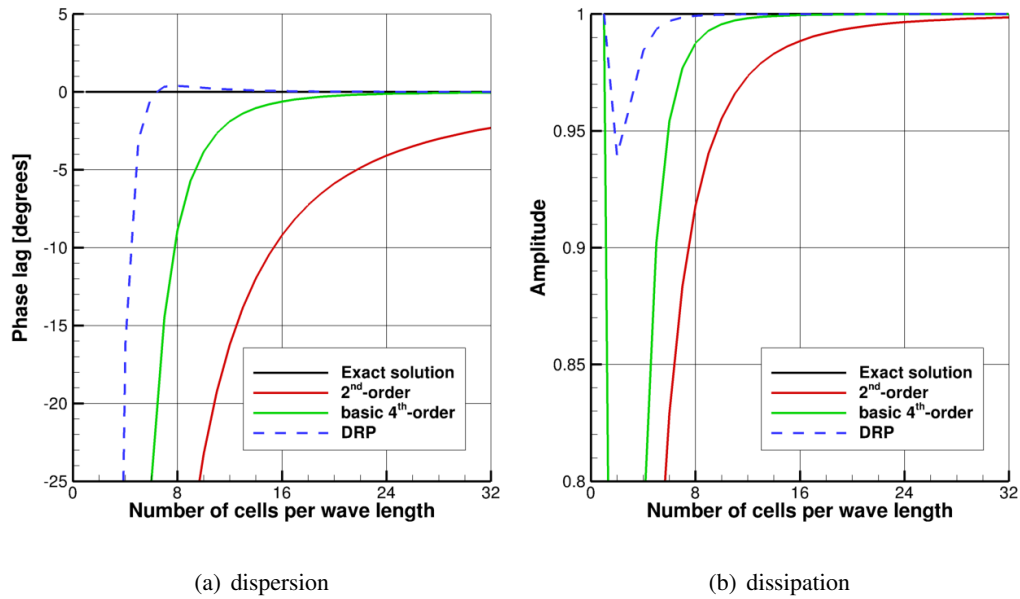


Fig. 1 Dispersion (phase lag) and dissipation (amplitude) for a single Fourier mode using different spatial discretizations and exact time integration

(see e.g. Verstappen and Veldman (Ref. 22)). Thus, kinetic energy is only dissipated by the sub-grid (and viscous) stresses and not by numerical errors. Furthermore, this implies that the numerical method is unconditionally stable for incompressible flow, without any artificial diffusion. For compressible flow, unconditional stability cannot be proven, but still stability is significantly enhanced, requiring only a very low level of artificial diffusion, if any. For compressible flow, sixth-order artificial diffusion is added to the equations (see reference 8), maintaining the fourth-order accuracy.

How much artificial diffusion is appropriate? This depends on the zone in a hybrid RANS–LES computation. In the RANS zones, very small mesh sizes are used to capture the boundary layers. Therefore, a second-order implicit time-integration method is typically used to avoid the strict stability limits of explicit schemes. The set of implicit equations per time step is solved with a multigrid scheme, requiring artificial diffusion for fast convergence. In the LES zones, however, such small mesh sizes are not present and artificial diffusion is not needed for rapid convergence.

An appropriate level of artificial diffusion for the LES zones was determined by considering the convection of an isentropic vortex on a strongly non-uniform grid (see reference 8 for the definition). Figure 2 shows the numerical error for three different levels of artificial diffusion, ranging from the ‘standard’ level used in RANS zones ($k^{(6)} = 2$) to the value found suitable for LES

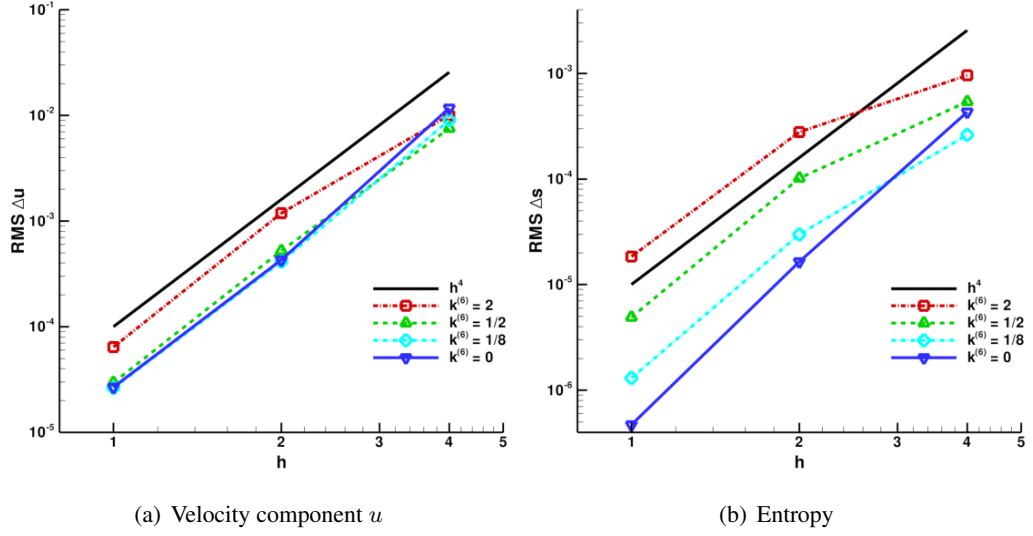


Fig. 2 Convection of isentropic vortex on strongly non-uniform grid: grid dependence of RMS value of difference with analytical solution of fourth-order low-dispersion symmetry-preserving scheme with and without sixth-order artificial diffusion

zones ($k^{(6)} = 1/8$), which is 16 times smaller. With the latter value, the error is not significantly increased compared to a computation without any artificial diffusion. Note that the computation is stable with such a low level of artificial diffusion (or even completely without it), thanks to the symmetry-preserving discretization.

Finally, the dissipation error can also be illustrated for the discretization of a linear, first-order transport equation using Fourier analysis, as shown in Figure 1(b). In this figure, the low-dispersion (DRP) scheme uses the LES-level of sixth-order artificial diffusion ($k^{(6)} = 1/8$), the basic fourth-order scheme uses the RANS-level of sixth-order artificial diffusion ($k^{(6)} = 2$), and finally the second-order scheme uses the RANS-level of fourth-order artificial diffusion (JST scheme (Ref. 6) with $\kappa^{(4)} = 1/32$). For the basic fourth-order and second-order schemes, point-to-point oscillations are damped by the same amount. With eight cells per wave length, the amplitude has decreased by only 0.1% for the low-dispersion (DRP) scheme, whereas it has decreased by 1% and 8% for the standard fourth-order and second-order schemes, respectively (factors 10 and 80 higher).

3.3 Time integration

The dissipation and dispersion errors due to the temporal discretization are often underestimated. The common practice is to determine the time step by the condition that the CFL number is one. In this section, we will show that with the standard time integration scheme used for DES

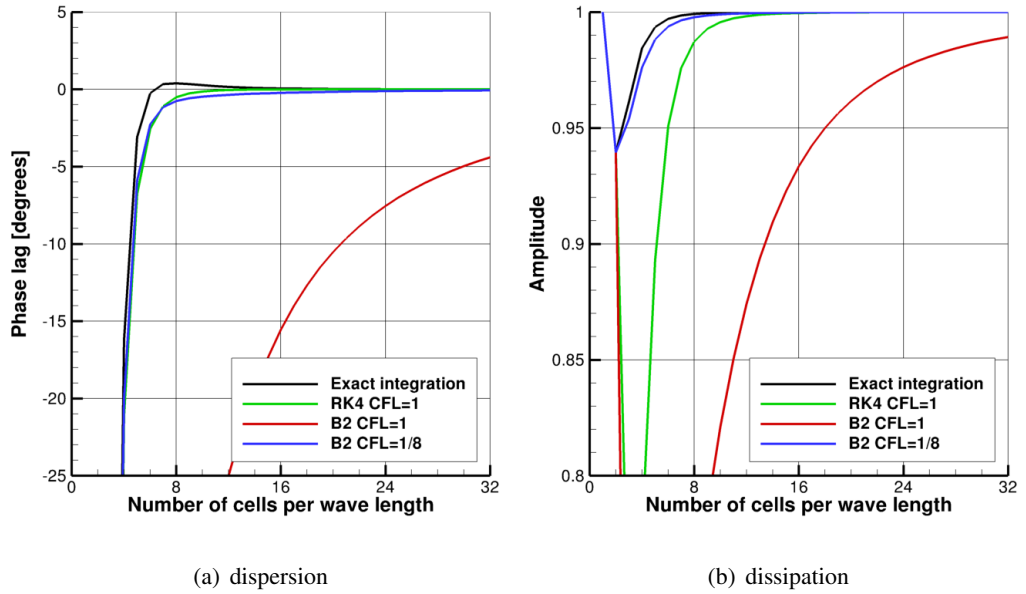


Fig. 3 Dispersion (phase lag) and dissipation (amplitude) for a single Fourier mode using the low-dispersion (DRP) scheme and different temporal discretizations

computations (second-order implicit) the resulting time step is too large and the temporal error swamps any good properties the spatial discretization may have.

Figure 3 shows the combined numerical errors of the low-dispersion finite-volume scheme of the previous section and two time integration schemes: the explicit Runge-Kutta 4 (RK4) method with $CFL = 1$ and the standard implicit two-point backward (B2) scheme with $CFL = 1$ or $CFL = 1/8$. The B2 scheme introduces significant numerical dispersion and dissipation if $CFL = 1$ is used, even more than the basic second-order spatial discretization (compare to Figure 1). With eight cells per wave length, it introduces an additional phase error of 46° and amplitude error of 26%. With $CFL = 1/8$, the error levels have become acceptable compared to the error of the spatial discretization: only 0.3° additional phase error and 0.1% additional amplitude error.

4 Results

4.1 Plane free shear layer

As a basic test case for investigating the stability issue, the experiment of Delville (Ref. 3) for a plane free shear layer is considered. The free shear layer starts from the trailing edge of a flat plate with free-stream velocities $u_1 = 41.54$ m/s and $u_2 = 22.40$ m/s at the different sides of the

flat plate and with fully developed turbulent boundary layers at the trailing edge. The Reynolds number based on the momentum thickness at the high-speed side is $Re_\theta = 2900$ at the trailing edge. The shear layer develops in a $0.3 \text{ m} \times 0.3 \text{ m}$ square test section of length 1.2 m . A self-similar flow with fully developed turbulence is reached well within the test section.

A computational domain is used with a length of 2.5 m (x -direction), a width of 0.15 m (z -direction) and a height of 0.3 m (y -direction). A computational ‘test section’ is defined with a length of $L = 1 \text{ m}$ after the trailing edge and with a uniform grid in the x - and z -directions. The grid has 1.29 million cells, with a mesh size $h = 3.125 \text{ mm}$ in the test section. The fourth-order, low-dispersion, symmetry-preserving finite-volume method is used with the levels of artificial diffusion set to $k^{(6)} = 2$ in the RANS zone and to $k^{(6)} = 1/8$ in the LES zone. Time steps are taken of size $\delta t = 9.6 \cdot 10^{-6} \text{ s}$, implying a convective CFL number, based on the maximum velocity u_1 , equal to $\text{CFL} = u_1 \delta t / h = 1/8$.

For an original X-LES computation (standard SGS model and numerics), the development of the shear layer is strongly delayed and the solution even remains 2D (Figure 4(a)). The solution essentially displays the behaviour of an initially laminar shear layer: growth of a 2D Kelvin–Helmholtz instability followed by vortex pairing.

Using the stochastic SGS model in X-LES, results in a dramatic improvement (Figure 4(b)). The initial, spanwise vortices appear much closer to the trailing edge and already show 3D disturbances. The flow then rapidly develops fully 3D turbulence. Comparison with experiment, however, is not fully satisfactory. In the experiment, the initial shear layer thickens much more rapidly and the growth rate is significantly lower further downstream (Figure 5(a)). Also the level of resolved Reynolds shear stresses is overpredicted (Figure 5(c)).

Further improvement is obtained with the HPF SGS model. The initial disturbances start even closer to the trailing edge and finer turbulent structures are captured further downstream (Figure 4(c)). Furthermore, the shear layer now displays the correct growth rate compared to the experiment and also the level of resolved Reynolds shear stresses compare well to the experiment (Figure 5).

The importance of accurate numerical schemes for capturing free shear layers is shown in Figure 4(d) and Figure 6. Additional computations with the stochastic HPF X-LES method have been performed with an increased level of artificial diffusion in the LES zones ($k^{(6)} = 2$) and/or an increased time step ($\text{CFL} = 1$). Clearly, the fine-scale turbulent structures are completely dissipated by the higher levels of numerical dissipation. As a consequence, the shear layer no

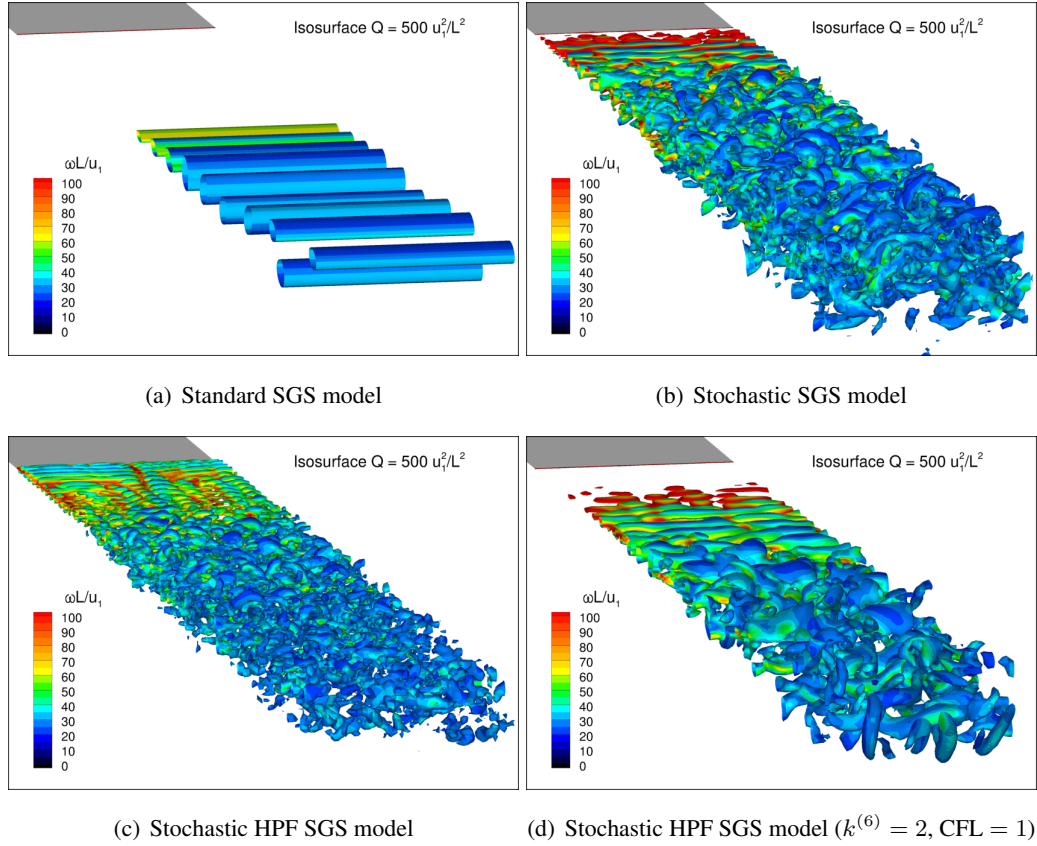
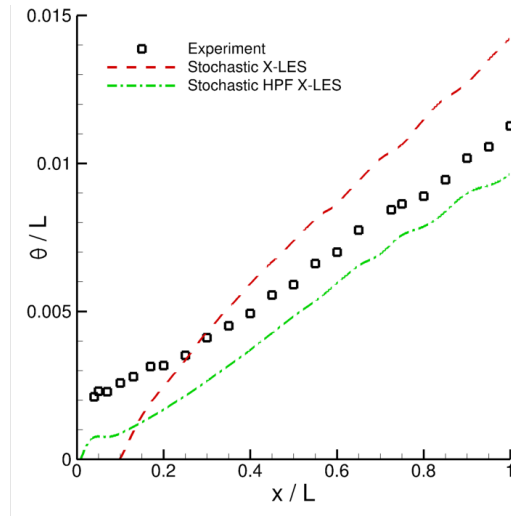


Fig. 4 Instantaneous isosurfaces of $Q = \Omega^2 - S^2$, coloured with vorticity magnitude Ω , for X-LES computations of plane free shear layer

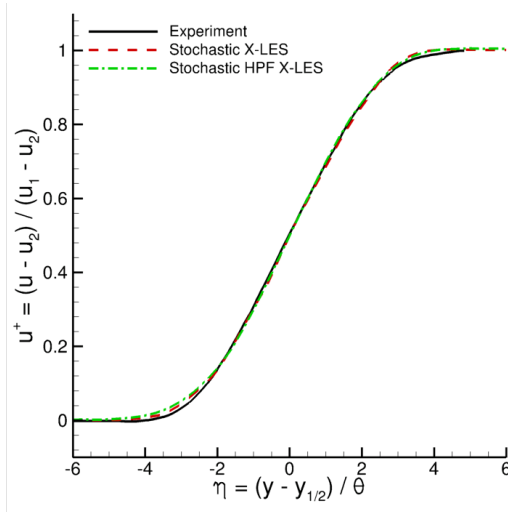
longer exhibits the correct growth rate. The energy spectrum rapidly starts to decay (and deviate from the experiment) at much lower frequencies, showing that the dissipation of kinetic energy is determined by the numerics instead of the SGS model. Using a convective CFL = 1, as is commonly done in DES-type computations, introduces more numerical dissipation than using the RANS-level of artificial diffusion (which was also shown by Figures 1 and 3). Note that the LES-level of artificial diffusion can only be used thanks to the enhanced stability of the symmetry-preserving discretization; a non-symmetry-preserving scheme would require a significantly higher level of artificial diffusion to remain stable.

4.2 Delta wing with sharp leading edge

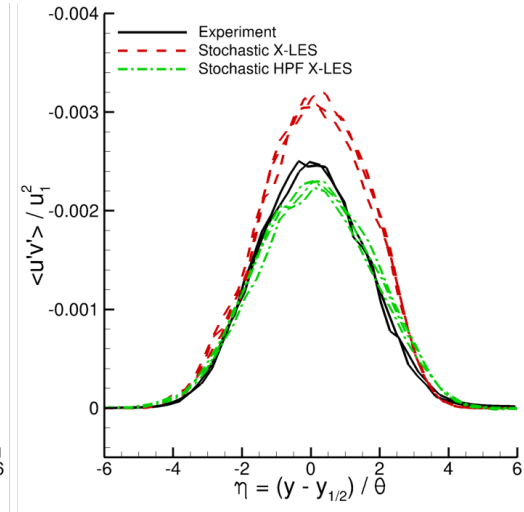
As a more challenging application, the flow around a delta wing with a sharp leading edge at high angle of attack and high Reynolds number is considered. This flow is characterized by the main vortex developing above the wing. The vortex is formed as the shear layer emanating from the leading edge rolls up, starting immediately at the apex. At high Reynolds numbers, the shear



(a) Momentum thickness



(b) Mean velocity profile



(c) Resolved Reynolds shear stress

Fig. 5 Time-averaged solution for X-LES computations of plane free shear layer

layer rapidly becomes unstable and a turbulent vortex is formed. At a sufficiently high angle of attack, the vortex breaks down: the high axial velocity in the vortex core drops rapidly to a value close to zero. To properly capture this flow, it is essential to capture the shear layer separating from the leading edge. In particular, the instability of this shear layer must be captured.

The NASA delta wing geometry of Chu and Luckring (Ref. 1) is considered, for which experiments that include measurements of velocity fluctuations have been performed by Furman and Breitsamter (Refs. 4, 5). Vortex breakdown occurs at the flow conditions $M = 0.07$, $Re_{\text{mac}} = 1 \cdot 10^6$, and $\alpha = 23^\circ$ (with the Reynolds number based on the mean aerodynamic chord c_{mac}).

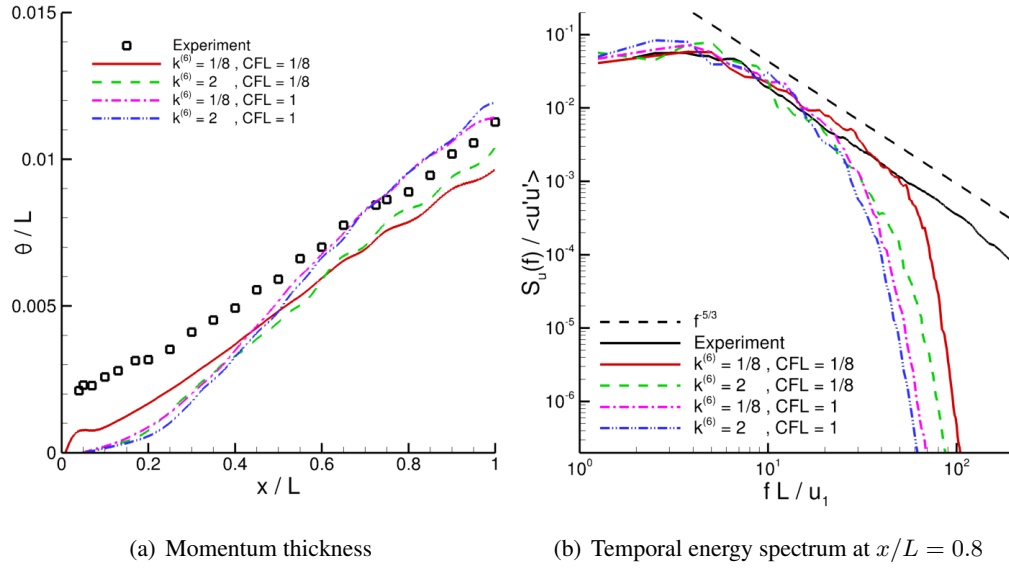


Fig. 6 Stochastic HPF X-LES computations of plane free shear layer with different levels of artificial diffusion ($k^{(6)}$) and different convective CFL numbers

A multi-block structured grid has been generated, consisting of 22 blocks and 6.3 million grid cells. The grid has a conical structure over a large part of the wing: the grid covering the main vortex is essentially isotropic at each chordwise station (outside the boundary layer) and the mesh width grows in all directions (including the streamwise direction) together with the main vortex, going from approximately $0.003c_{mac}$ to $0.011c_{mac}$. In other words, the grid resolution relative to the main vortex is kept constant. Only in a small region near the apex, the conical structure is not fully maintained, avoiding a grid singularity. The far-field boundary is located at three root chord lengths from the wing. To study grid sensitivity, also a finer grid with the mesh width reduced by a factor 2/3 in all directions (21.4 million grid cells) has been generated.

Computations have been performed with stochastic HPF X-LES and delayed HPF X-LES, as well as with standard SST-DDES as reference, all using the same optimized numerical method and the same time step (again corresponding to a convective $CFL = 1/8$). The delayed HPF X-LES method does not include the stochastic SGS model, but it does include the shielding function of DDES (Ref. 21) that protects attached boundary layers from inadvertently switching to LES mode. An impression of the instantaneous results is given in Figure 7. Including the delayed approach in X-LES leads to the suppression of the LES mode in a weakly separated region in the wing/sting corner; otherwise, the solutions of the two HPF X-LES computations are the same. Compared to SST-DDES, HPF X-LES is able to capture significantly finer turbulent structures. Furthermore the primary vortex and the shear layers remain stable over a large part of the

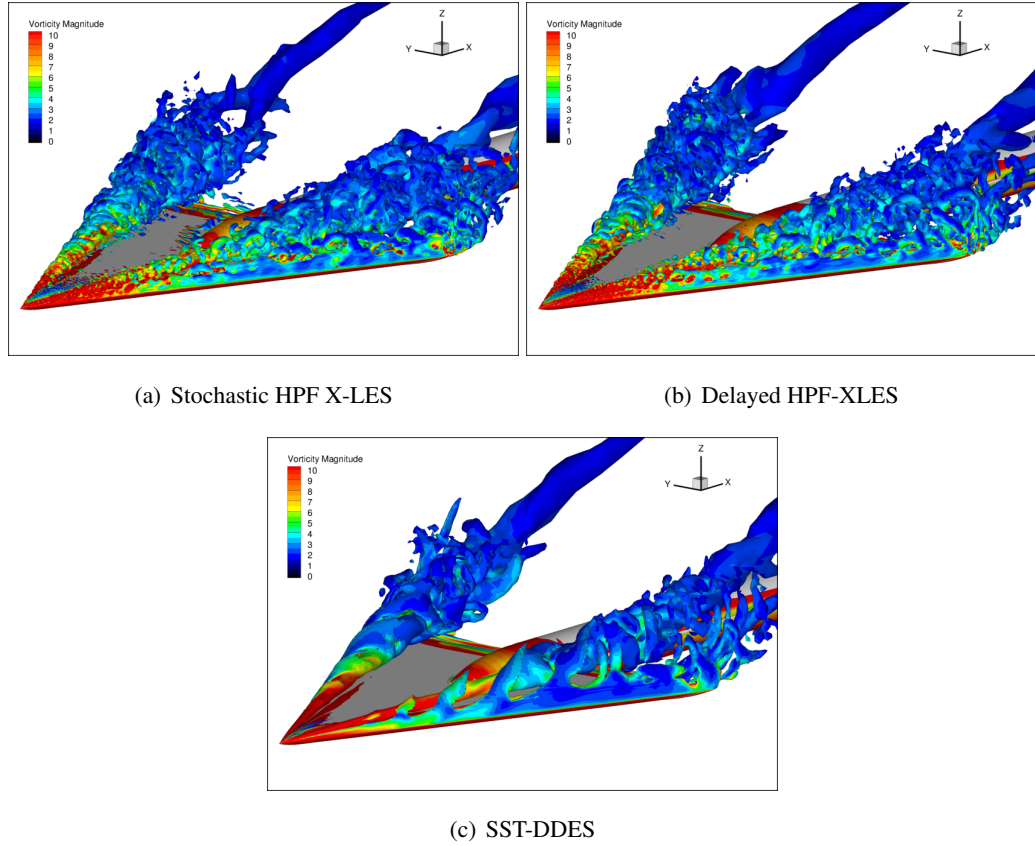


Fig. 7 Instantaneous isosurfaces of $Q = \Omega^2 - S^2$, coloured with vorticity magnitude Ω , for DES-type computations of flow around a delta wing with sharp leading edge

wing for SST-DDES, in contrast to HPF X-LES. This difference between X-LES and SST-DDES is most likely attributable to the HPF SGS model (and not to the stochastic SGS model, which is not included in delayed HPF X-LES).

Figure 8 compares the level of resolved turbulent kinetic energy of the computations to the experiment at a constant plane $x/c_r = 0.4$ (with c_r the root chord). Clearly, the SST-DDES computation strongly underpredicts the level of turbulent kinetic energy, as the solution is practically steady in this region. In contrast, the delayed HPF X-LES computation shows a level of turbulent kinetic energy that is comparable to the experimental result. On the fine grid, practically the same result is obtained, showing the weak dependence of the X-LES solution on the grid resolution.

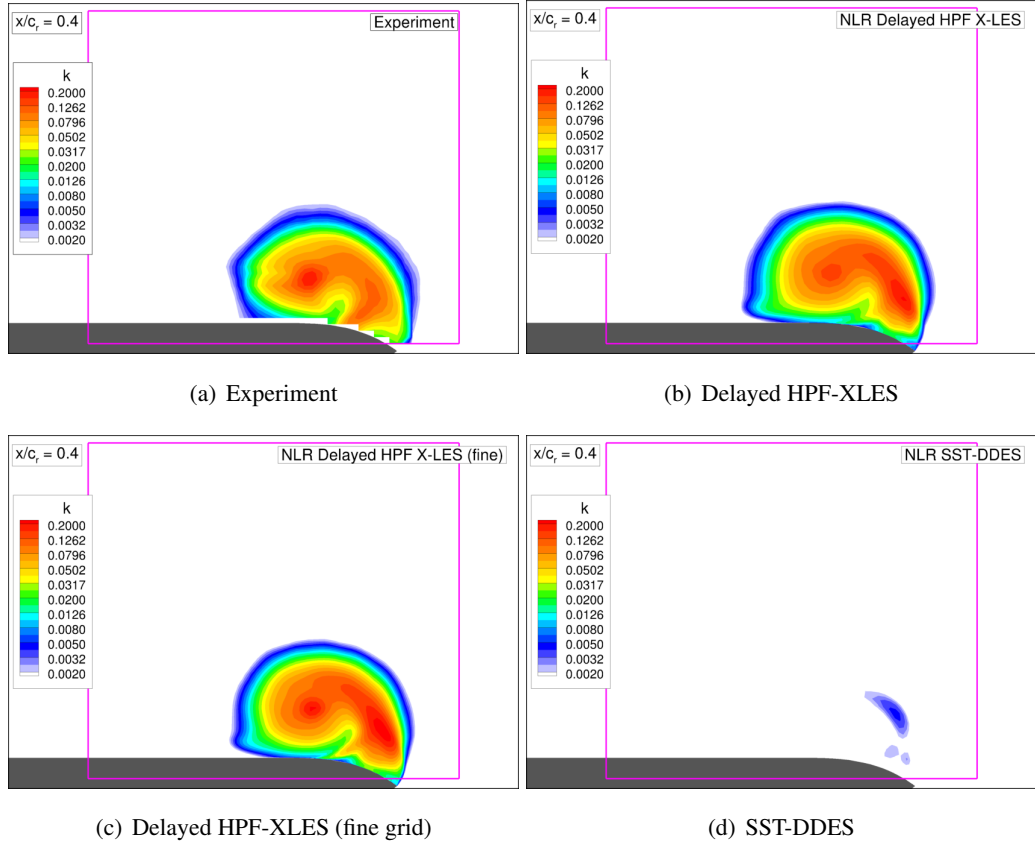


Fig. 8 Resolved turbulent kinetic energy at plane $x/c_r = 0.4$ for the experiment and for DES-type computations of flow around a delta wing with sharp leading edge

5 Conclusions

Capturing free shear layers in DES-type computations can be substantially improved using modifications of the SGS model. These modifications are non-zonal and do not require knowing the separation location *a priori*. Shear-layer instabilities can be triggered by including a stochastic SGS model. A correct growth rate of the shear layer can be obtained by using a high-pass filtered (HPF) SGS model that reduces the level of subgrid stresses at the onset of the free shear layer.

Numerical methods must be carefully designed in order to accurately capture free shear layers without numerical errors overwhelming the subgrid stresses. In particular, a fourth-order, low-dispersion, symmetry-preserving finite-volume method has been used. The symmetry-preserving discretization ensures that computations are stable without any artificial diffusion for incompressible flow and with only a low level of artificial diffusion for compressible flow. Thus, kinetic energy is dissipated by the subgrid stresses and not by numerical errors.

Finally, one needs to be careful with the second-order implicit time integration commonly used for DES computations. With a time step corresponding to a convective CFL number equal to one, the time integration is much too dissipative and the temporal discretization error swamps any good properties the spatial discretization may have. With a convective CFL number equal to $1/8$, the spatial and temporal discretization errors are balanced.

Acknowledgements

The research described in this paper is funded partly by the EU project ATAAC (Advanced Turbulent simulation for Aerodynamic Application Challenges) and partly by NLR's programmatic research 'Kennis als Vermogen'.

References

1. J. Chu and J. M. Luckring. Experimental surface pressure data obtained on 65° delta wing across Reynolds number and Mach number ranges. TM 4645, NASA, 1996.
2. S. Deck. Recent improvements in the zonal detached eddy simulation (ZDES) formulation. *Theoretical & Computational Fluid Dynamics*, 2011.
3. J. Delville. *La décomposition orthogonale aux valeurs propres et l'analyse de l'organisation tridimensionnelle de écoulements turbulents cisailés libres*. PhD thesis, Université de Poitiers, 1995.
4. A. Furman and Ch. Breitsamter. Turbulent and unsteady flow characteristics of delta wing vortex systems. In *46th AIAA Aerospace Sciences Meeting and Exhibit*, Reno (NV), USA, 7–10 January 2008. AIAA 2008-381.
5. A. Furman and Ch. Breitsamter. Experimental investigations on the VFE-2 configuration at TU Munich. In *Understanding and Modeling Vortical Flows to Improve the Technology Readiness Level for Military Aircraft*, chapter 21. NATO RTO, 2009. RTO-TR-AVT-113.
6. A. Jameson, W. Schmidt, and E. Turkel. Numerical solutions of the Euler equations by finite volume methods using Runge–Kutta time-stepping schemes. In *14th Fluid and Plasma Dynamics Conference*, Palo Alto, CA, June 23–25 1981. AIAA-1981-1259.
7. N. Jarrin, S. Benhamadouche, D. Laurence, and R. Prosser. A synthetic-eddy-method for generating inflow conditions for large-eddy simulations. In *1st Hybrid RANS–LES Symposium*, Stockholm, Sweden, 14–15 July 2005.
8. J. C. Kok. A high-order low-dispersion symmetry-preserving finite-volume method for compressible flow on curvilinear grids. *Journal of Computational Physics*, 228:6811–6832, 2009. NLR-TP-2008-775.

9. J. C. Kok, H. S. Dol, B. Oskam, and H. van der Ven. Extra-large eddy simulation of massively separated flows. In *42nd AIAA Aerospace Sciences Meeting*, Reno, NV, 5–8 January 2004. AIAA paper 2004-264.
10. J. C. Kok and H. van der Ven. Destabilizing free shear layers in X-LES using a stochastic subgrid-scale model. In S. H. Peng, P. Doerffer, and W. Haase, editors, *Progress in Hybrid RANS–LES Modelling*, volume 111 of *Notes on Numerical Fluid Mechanics and Multidisciplinary Design*, pages 179–189. Springer, 2009. NLR-TP-2009-327.
11. A. G. Kravchenko and P. Moin. On the effect of numerical errors in large eddy simulations of turbulent flows. *Journal of Computational Physics*, 131:310–322, 1997.
12. S. K. Lele. Compact finite difference schemes with spectral-like resolution. *Journal of Computational Physics*, 103(1):16–42, 1992.
13. M. Lesieur and O. Métais. New trends in large-eddy simulations of turbulence. *Annual Review of Fluid Mechanics*, 28:45–82, 1996.
14. E. Lévéque, F. Toschi, L. Shao, and J.-P. Bertoglio. Shear-improved smagorinsky model for large-eddy simulation of wall-bounded turbulent flows. *Journal of Fluid Mechanics*, 570:491–502, 2007.
15. M. L. Shur, P. R. Spalart, and M. Kh. Strelets. Noise prediction for increasingly complex jets. Part I: Methods and tests. *International Journal of Aeroacoustics*, 4(3&4):213–246, 2005.
16. M. L. Shur, M. Kh. Strelets, and A. Travin. On the role of numerics on detached eddy simulation. In P. Neittaanmäki, T. Rossi, S. Korotov, E. Oñate, J. Périaux, and D. Knörzer, editors, *ECCOMAS 2004*, Jyväskylä, Finland, 24–28 July 2004.
17. P. R. Spalart. Detached-eddy simulation. *Annual Review of Fluid Mechanics*, 41:181–202, January 2009.
18. P. R. Spalart, W.-H. Jou, M. Strelets, and S. R. Allmaras. Comments on the feasibility of LES for wings, and on a hybrid RANS/LES approach. In C. Liu and Z. Liu, editors, *Advances in DNS/LES*. Greyden Press, 1997. Proc. 1st AFOSR Int. Conf. on DNS/LES, 1997, Ruston (LA), USA.
19. S. Stolz. High-pass filtered eddy-viscosity models for large-eddy simulations of compressible wall-bounded flows. *Journal of Fluids Engineering*, 127:666–673, July 2005.
20. C. K. W. Tam and J. C. Webb. Dispersion-relation-preserving finite difference schemes for computational acoustics. *Journal of Computational Physics*, 107:262–281, 1993.
21. A. K. Travin, M. L. Shur, P. R. Spalart, and M. Kh. Strelets. Improvement of delayed detached-eddy simulation for LES with wall modelling. In P. Wesseling, E. Oñate, and J. Périaux, editors, *ECCOMAS CFD 2006*, Egmond aan Zee, The Netherlands, 5–8 September 2006.

22. R. W. C. P. Verstappen and A. E. P. Veldman. Symmetry-preserving discretization of turbulent flow. *Journal of Computational Physics*, 187(1):343–368, 2003.